Simulation of Multi-deck Medium Temperature Display Cabinets with the Integration of CFD and Cooling Coil Models

Y.T. Ge*   S.A. Tassou   A. Hadawey

Mechanical Engineering, School of Engineering and Design, Brunel University,

Uxbridge, Middlesex, UB8 3PH, UK

ABSTRACT

In this paper, the model for the multi-deck medium temperature display cabinets is developed with the integration of CFD and cooling coil sub-models. The distributed method is used to develop the cooling coil model with the airside inputs from the outputs of the CFD model. Inversely, the airside outputs from the cooling coil model are used to update the boundary conditions of the CFD model. To validate this cabinet model, a multi-deck medium temperature display cabinet refrigerated with a secondary refrigerant cooling coil was selected as a prototype and mounted in an air conditioned chamber. Extensive tests were conducted at constant space air temperature and varied relative humilities. The cabinet model has been validated by comparing with the test results for the parameters of air at different locations of the flow path, and temperatures of refrigerant and food product etc. The validated model is therefore used to explore and analyze the cabinet performance and control strategies at various operating and design conditions.

Keywords: integrated display cabinet model, CFD, cooling coil, test, model validation and application.

* Corresponding author. Tel.:+44 1895 266722; fax: +44 1895 256392.
E-mail address:yunting.ge@brunel.ac.uk

Nomenclature

A	area (m^2)	*Subscripts*	
a	absorption coefficient	a	air
b	scattering coefficient	a, sen	air sensible
C_p	specific heat at constant pressure ($J\ kg^{-1}k^{-1}$)	i	inner
C	capacity rate ($W\ k^{-1}$)	min	minimum
d	diameter(m)	o	outer
h	enthalpy($J\ kg^{-1}$)	r	refrigerant
Hum	air humidity (%)	tot	total
Humamb	space air humidity (%)	w	wall
I	radiation intensity (W/m^2)	wi	inner wall
i, j, k	coordinates		
k	turbulent kinetic energy ($m^2\ s^{-2}$)		
Le	Lewis number		
$\dot{m}$	mass flow rate ($kg\ s^{-1}$)		
P	pressure (Pa)		
$\dot{q}$	heat transfer per square meter ($W\ m^{-2}$)		

$\dot{Q}$ heat transfer (W)

R resistance (k W^{-1})

R_k source term of k (kg m^{-1}s^{-3})

R_ε source term of ε (kg m^{-1}s^{-4})

s perimeter of inner pipe (m), direction

T temperature (k)

$Tamb$ space air temperature (°C)

u velocity component in x-direction , velocity (m s^{-1})

v velocity component in y-direction (m s^{-1})

UA overall heat transfer coefficient (W k^{-1})

U_m mass transfer coefficient (kg s^{-1}m^{-2})

Vel_air cabinet air velocity (m/s)

w solid angle (rad)

x horizontal coordinate (m)

y vertical coordinate (m)

z   length (m)

α heat transfer coefficient (W m^{-2}k^{-1})

Γ_k diffusion coefficient of k

Γ_ε diffusion coefficient of ε

ε dissipation rate of turbulent kinetic

energy (m^2 s^{-3}); effectiveness

η efficiency

Δ difference

ρ density (kg m^{-3})

τ shear stress (N m^{-2})

ω   humidity ratio

1. Introduction

The medium temperature multi-deck refrigerated display cabinet is extensively installed in a supermarket refrigeration system due to its function and convenient accessibility. A typical supermarket may have over a 100m length of such display cabinets, altogether contributing significantly to its total energy consumption. The energy consumption of a typical supermarket in the UK is approximately 1000 kWh/m^2, of which about 40% to 50% will be used for refrigeration purposes [1]. The multi-deck display cabinets require around 70% of this refrigeration energy and, consequently, could be responsible for annual carbon emissions of between 100 and 130 kg CO$_2$/m^2 sales area. With over 6000 supermarkets in the UK acquiring an average area of 1700 m^2, the multi-deck display cabinet in supermarkets in the UK may be accountable for the 1.2 million tonnes of CO$_2$ emissions per year [2]. Accordingly, this type of display cabinet will be investigated in this paper.

More than 70% of the total cabinet cooling capacity is prerequisite in covering the moist and warm air infiltration through the open front air curtain. However, an innovated air curtain design and operation to heighten its efficiency can fundamentally reduce the total cooling load and ultimately save energy from the compressor packs. Certain structure and operating parameters can also affect the performance of the air curtain, including the width of discharge air grill, discharge air temperature, velocity

magnitude and profile, turbulence intensity, internal and external space air conditions, and back panel flow etc. Therefore, the purely experimental means of exploration into these effect parameters proves exceedingly difficult and possibly unachievable. A validated CFD model is the paramount choice for the prediction and analysis of air flow, from the cooling coil air-off to the air-on in the sequence of the back panel flow and the case top air channel flow to the air curtain discharge and air curtain. This CFD model can essentially replace the experiment, depending on the accuracy of the specified boundary conditions at the cooling coil air-off.

In the case of the application of a secondary refrigerant, the cooling coil, as opposed to the evaporator, will determine the total cooling capacity required by the cabinet. A detailed and accurate cooling coil model can produce the reliable boundary parameter profiles necessary for the CFD model, including air temperature and humidity. Alternatively, the outputs of the precise CFD model can be used as input parameter profiles for the detailed cooling coil model. Therefore, an integration of the CFD and cooling coil models prove to be more adequate in the simulation and analysis of the cabinet performance to ultimately optimize both its design and operation. However, to the authors' knowledge, there is no integrated CFD and cooling coil model in public literature liable for use in the cabinet simulation. In other words, the concentrations of previous research in this area have either been focused solely upon the CFD models or the cooling coil models.

A thorough and significant study into the performance of the vertical types of air curtains was conducted, even before the CFD technique was widely employed in this area [3-5]. They related the air curtains' performance quantitatively to major parameters such as the opening height, discharge air grille (DAG) width, jet velocity, and

turbulence intensity at the DAG. These parameters are crucial to a thorough comprehension of the operating behaviour of such air curtains. For the simulation of the air curtains, a comprehensive model based upon the finite difference technique was presented [6]. The results from this simulation were exploited to produce simplified correlations in the prediction of air curtain performance. It is understood that, by means of CFD technology, more detailed and accurate models for simulating the performance of the display cabinet air curtains (DCAC) can be accomplished [7]. The thermal performance and fluid dynamics of DCACs were simulated with 2-D steady state CFD model and tested in the laboratory with its air flow routine commencing through the evaporator air-off, back panel flow and air curtain before returning to the evaporator air-on [8]. This simulation observed that the turbulence intensity at the DAG greatly affected the degree of air entrainment to the air curtain, and a reduction could be implemented by means of modifying the honeycombs at the DAG. Another 2-D CFD model was developed to predict the air flow pattern and food temperature of different types of display cabinets [9]. In the mean time, the influence of warm air infiltration on the energy balance of the cabinets was investigated and it was found that the air curtain discharge air velocities were important factors to affect the curtain efficiency. The work was further developed to apply 3-D CFD model into the cabinet simulation after verified that the extremity effects caused by the side walls were quite important particularly for the shorter cabinets which could not be detected by the 2D model [10]. The jet velocity was also a dominated parameter affecting the effectiveness of air curtain applied in cold room entrance and could be optimised by means of a 3-D CFD model [11]. Furthermore, with the help of the 3-D CFD model, the food product

6

The ambient air entrainment is the principal reason for the large infiltration loss in the air curtains. To investigate this discovery more thoroughly, the ambient air entrainment in refrigerated display cabinets was exploited using CFD modelling with experimental techniques from the Digital Particle Image Velocimetry (DPIV) to study the flow and temperature field characteristics of the air curtains [13]. Further works were aimed at addressing, in more detail, the influence of the cabinet and air curtain design parameters on air entrainment [14][15]. The results illustrated that a reduction in turbulence intensity significantly affected low Reynolds numbers at the discharge grille, although Reynolds numbers above 3200 initial turbulence intensity had little effect upon the ambient air entrainment.

The main differences between the cooling coil and evaporator models are manifest in refrigerant side conservation equations and heat transfer calculations, since the former employs secondary refrigerants such as propylene glycol/water and the latter primary refrigerant such as R404A etc. However, there is no difference evident in the air side calculations in the application of the same type of heat exchanger such as finned-tube. A model for simulating a finned-tube display case evaporator was developed with the expectation for the model to be used as a design tool to implement the improvement of evaporator performance at different frosting conditions [16]. The various states of the evaporator air inlet were determined by the designed airflow rates and fixed loads although the actual methods to determine and calculate the loads were not given in the paper. Similarly, modelling and experimental analyses for a finned-tube evaporator used in low temperature frozen food display cabinet were conducted [17]. Base on lump

method, the model was developed to investigate the influence of indoor conditions on the performance of the display cabinets and able to predict frost thickness and effectiveness of display cabinet heat exchangers. Another finned-tube air-cooling evaporator model was built which was based upon the tube-by-tube distributed method in order to suit the simulation of heat exchangers with different circuit designs [18]. The model was validated with the test results for refrigerants R22 and R410A although the refrigerant evaporating temperatures employed in the tests were constantly above 0°C such that the accumulation of frost upon the outer surface of the heat exchanger was not taken into account. Alternatively, the dynamic behaviour of frost formation in the finned-tube evaporator was studied along with the development of a dynamic distributed model, which attained several meaningful results, including frost development and its effect upon energy and mass transfers[19]. A dynamic finned-tube evaporator model of a refrigeration system was developed, of which a novel iteration method to minimise the simulation time was proposed [20]. It suggested that the modelling of the evaporator based on distributed method be more accurate comparing with that utilising lump method.

An integration of the CFD and cooling coil model is developed in this paper to simulate and analyse the performance of the multi-deck medium temperature display cabinet. The 2-D CFD model can predict the air dynamics of air flow, heat and mass transfer among the air flow, food products and ambient space air. The air flow covers the routine through the cooling coil air-off, back panel flow to the air curtain and back to the cooling coil air-on. The distributed method is employed to model the finned-tube cooling coil such that different pipe and fin structures and circuit arrangements can be simulated, with the outputs from the cooling coil model used as the inputs to the CFD

model and vice versa. To validate this integration model, a typical multi-deck medium temperature display cabinet was selected as a prototype and mounted into an air conditioned chamber. Extensive experiments were conducted at the conditions of a constant chamber ambient air temperature and varied relative humidity, together with the validation of an integrated model by comparing the simulation with the test results. The validated model is therefore used to examine the cabinet performance and explore the optimal control strategies at various operating conditions, including total air flow rates and space air parameters etc.

2. Descriptions of the Display Cabinet

The Carter multi-deck medium temperature display cabinet shown in Figure 1 was selected as a prototype for the experiment and model validation, with a secondary refrigerant (40% mass propylene glycol/water) cooling coil mounted underneath. Propeller fans were also installed before the cooling coil in order to force the air flow into circulating around the cabinet. The refrigerated air flow from the cooling coil air-off would first enter the back panel flow tunnel before instantly penetrating into the case inside through the perforated back panel, and subsequently approaching the discharge air grill to commence the air curtain path, and afterward flowing into the return air grill before finally pouring back into the cooling coil air-on.

The main structure data of the cabinet is outlined below:

- There are five product shelves from top to bottom of the cabinet.

- The distance from the cabinet ceiling to the top shelf is 250 mm while the gap between the fourth and bottom shelves is 350 mm.

- The top shelf is 870 mm above the fourth shelf and this distance is evenly divided by the 2nd and 3rd shelves.

- The front opening height of the display cabinet is 1450 mm.

- The designed perforate rate of the perforated back panel is constant at 4.5 % for the panel above the fourth shelf and at 0.8% below.

- The gapes of back and top panel flow tunnels are 45 mm and 65 mm respectively.

Figure 1 Tested Carter display cabinet

The cooling coil is a type of finned-tube heat exchanger with the secondary refrigerant flowing inside the tube and air passing externally. A side view of the coil is shown in Figure 2 , with 4 pipe circuits at 8 pipes each, amounting to a total of 32 pipes. The refrigerant is flowing in a left-to-right direction whilst the air is flowing opposite, leading to an approximate counter-flow. The dimensions of the coil are:

- Length of 2.1m along the pipes;

- Height of 0.14m in the transverse direction;

- Depth of 0.35 m in the longitudinal direction;

- The pipe outer and inner diameters of 19.05mm and 18.05mm respectively;

- The pipe spacing of 60mm in the longitudinal direction and 25 mm in the transverse direction;

- The fin spacing of 12mm for the first two rows from the air-on and 6mm afterward;

- The fin thickness of 0.2 mm with a flat pattern.

Figure 2. The cooling coil in the tested display cabinet

3. Experimental Setup

The experiment design and setup adhered to the guidelines specified in the European Standard EN441 1995. The display cabinet test facility was comprised of an environmental chamber, an air conditioning system to maintain temperature and relative humidity within the chamber, the tested display cabinet described in Section 2, and a data acquisition system. All tests were performed under steady-state conditions wherein the environmental chamber was controlled at a constant dry-bulb temperature and a constant relative humidity over the test period for a minimum of 24 hours. To maintain these two space air parameters, the conditioned air flow was designed for 100% re-circulation and the display cabinet as described in Section 2 was instrumented and mounted inside the conditioned chamber. The shelves of the cabinet were loaded with either product simulators (30% cellulose, 70% water and salt) or water containers at similar thermal capacities.

During these test periods, the several important parameters measured and recorded included: the space air temperature and relative humidity inside the chamber, the secondary refrigerant inlet and outlet temperatures, refrigerant mass flow rate and pressure drop through the cooling coil, air temperatures and relative humidity at the air-on and air-off of the cooling coil, circulated air velocity at the back flow tunnel inlet, and the product temperatures. The product temperatures were measured solely at the product simulators, which were loaded upon the shelves at the top, tertiary and bottom levels, as shown in Figure 3. On each shelf, there were six packs of product simulators placed on the left, middle and right at both front and rear edges. For each product simulator, a thermocouple was inserted into the centre to measure the average temperature of the product.

The specifications of the sensors used in these measurements are listed in Table 1. All sensors were calibrated before undertaking the measurement of the data, which was sampled every 10 seconds by the data acquisition system, and saved onto a data file every 60 seconds to be processed shortly afterwards.

Figure 3. Locations of product simulators inside the display cabinet

Table 1. Specifications and data descriptions of sensors used in the experiment

4. Model description

4.1 CFD model

The commercial CFD software, Fluent 6.3, was employed for the development of the 2D steady-state CFD model to simulate the cabinet air flow dynamics from the cooling coil air-off to the air-on. The standard k-ε two-equation model [21], as shown in Equations (1) and (2), was used as the turbulent model whilst the discrete ordinates model was applied as the radiation model (3)[22]. The implementation in Fluent of the radiation model used a conservative variant called the finite-volume scheme and its extension to unstructured meshes. Since the moist air in the air flow contained two mixing species of dry air and water, the species calculation was conducted using the species transport model. By solving simultaneously the species model with other conservation equations, the fields of temperature and humidity ratio in the domain could be predicted such that the air relative humidity would be calculated accordingly. It is noted that water condensation on the surfaces of the cabinet was not considered in the model. A non-uniform calculation grid with the total grid number 12192 was produced in the calculation domain, as shown in Figure 4, along with various trial calculations to verify that not effect of further grid number increase upon the calculation accuracy. To ensure the model accuracy, the grid densities near walls and shelves were purposely increased with particular mesh schemes. The SIMPLE algorithm [23] was employed as the solution method for the pressure-velocity coupling, with the boundary condition setup as the main task for CFD modelling. In the CFD model, the calculation domain acquired the entire midway cross-section of the conditional chamber in which the tested cabinet was located, as shown in Figure 4. Moreover, the boundary conditions of two side walls of the chamber (left and right) were defined as a pressure inlet and pressure

13

outlet respectively and for each wall, the boundary temperature was used to specify for the external black body temperature and the internal emissivity was assumed constant. The various associated parameters, including thermal and species, were obtained from the measurements and those of turbulence data from assumptions. The ceiling and floor of the chamber were defined as adiabatic walls, and boundary conditions of the coil air-off and air-on defined as a velocity inlet and pressure outlet respectively. In addition, the boundary condition of the cold perforated back panel was set as porous jump in which the face permeability was correlated as constant from measurement. Furthermore, the associated parameters of the velocity inlet applied from the measurements would later be replaced by the outputs of the cooling coil model. The perforated back panel was defined as a porous jump condition of which the parameters can be adjusted according to the panel perforated rate, whilst the rest of surfaces were all classified as walls with coupled thermal conditions.

$$\frac{\partial(\rho u k)}{\partial x} + \frac{\partial(\rho v k)}{\partial y} = \frac{\partial}{\partial x}(\Gamma_k \frac{\partial k}{\partial x}) + \frac{\partial}{\partial y}(\Gamma_k \frac{\partial k}{\partial y}) + R_k \tag{1}$$

$$\frac{\partial(\rho u \varepsilon)}{\partial x} + \frac{\partial(\rho v \varepsilon)}{\partial y} = \frac{\partial}{\partial x}(\Gamma_\varepsilon \frac{\partial \varepsilon}{\partial x}) + \frac{\partial}{\partial y}(\Gamma_\varepsilon \frac{\partial \varepsilon}{\partial y}) + R_\varepsilon \tag{2}$$

$$\frac{dI}{ds} + (a + b)I = a\frac{\sigma T^4}{\pi} + \frac{b}{4\pi}\int_0^{4\pi} I(s,w)dw \tag{3}$$

Figure 4 Computational grids for the 2D CFD model

4.2 Cooling coil model

The distributed method was employed in modelling the finned-tube air-cooling cooling coil, along with the use of a secondary refrigerant (40% mass propylene glycol/water). To clearly describe the modeling process via the application of the distributed method, a sample finned-tube heat exchanger is chosen here; with its side view diagram shown in Figure 5. This heat exchanger has one pipe circuit totaling 20 pipes: 4 pipe rows in the longitudinal direction with 5 pipes in each row. As shown in the above diagram:

- The refrigerant inlet is at the top-left;

- The refrigerant outlet is at the top-right;

- The dotted and solid lines represent the U-bend pipes at the rear and front sides respectively;

- The air flow direction is from right to left;

- The pipes are numbered in order from refrigerant inlet to the outlet;

- The pipe rows are numbered in order from air flow inlet to the outlet.

With the distributed modeling method, the heat exchanger necessitates a division into small elements wherein each element can be identified by its coordinate. The origin of the 3D coordinate is situated at the bottom-right pipe, No. 16, of the first pipe row in the front coil side. The i coordinate is the direction along the pipe length and the maximum i coordinate is dependent upon how many grids are divided along a pipe length. Hypothetically, the more grids present, the greater the accuracy of simulation results; but longer calculation time is expected. The j coordinate is numbered together with the pipe row number in the longitudinal direction, with the k coordinate from the bottom pipe in the transverse direction. A repetition of the above procedure would only occur if

15

another pipe circuit is inclusive within the heat exchanger. As a result, any division of small elements in the heat exchanger can be coordinated in a function of the pipe circuit number and pipe number in each circuit. The next step would be to establish the conservation equations for each element, and subsequently to efficiently solve these equations. The routine for resolving the equation commences primarily from the circuit loop, should there be more than one circuit for the coil. For each circuit, the simulation will run through each numbered pipe from the refrigerant inlet through to the element loop, whereby the solutions for one sub-element can be utilised as the inputs for the next sub-division. Initially, the typically unknown air side parameters for each element will be assumed, until these parameters are updated by the next iteration and the total cooling capacity of the cooling coil would be calculated at the end of each iteration. The iteration will continue until all the loops are cycled and the total cooling capacities for two continuous iterations remain practically unchanged.

Figure 5. A sample air-cooling heat exchanger and coordination of the divided small element

4.2.1 Refrigerant side conservation equations

Before ascertaining the refrigerant side conservation equations for each element, the following assumptions are proposed:

- The system is in a steady state.

- There is no heat conduction in the direction of the pipe axis and nearby fins.

- The air is of a homogeneous distribution, where there is an equal air-facing velocity to each element.

- There is no contact heat resistance between the fin and pipe.

- At all points in the flowing direction, the refrigerant is in thermal equilibrium.

Mass equation:

$$\frac{d}{dz}(\dot{m}_r) = 0 \tag{4}$$

Momentum equation:

$$\frac{1}{A_i}\frac{d}{dz}(\dot{m}_r u) = -\frac{dP}{dz} - \frac{\tau_{wi} s_{wi}}{A_{wi}} \tag{5}$$

Energy equation:

$$\frac{d}{dz}(\dot{m}_r h) = (\pi d_o)\dot{q} \tag{6}$$

The above equations can be easily discretized for a sub-element node at (i, j, k) with the grid size of $\Delta z_i \times \Delta z_j \times \Delta z_k$, as shown in Figure 5. Therefore, the refrigerant parameters at ($i+1$, j, k) can be solved.

These conservation equations can also be applied for the airside calculation, where the pressure drop calculation would be used as a replacement for the momentum equation, with the heat transfer calculation inclusive within the overall energy equation. In addition, a heat balance between both the air and refrigerant sides is manifest for each element.

4.2.2 Airside Heat Transfer

The Number of Transfer Unites-effectiveness (*NTU-ε*) Method is employed in the sensible heat transfer calculation for the airside in one grid section. The *NTU-ε* Method is used to calculate the rate of heat transfer in heat exchangers when there is insufficient information to calculate the Log-Mean Temperature Difference [24].

$$\dot{Q}_{a,sen} = \varepsilon C_{\min}[T_a(i,j,k) - T_r(i,j,k)] \tag{7}$$

The overall heat transfer coefficient can be calculated as follows:

$$UA = (\frac{1}{\alpha_a \eta_o A_o} + \sum R_i + \frac{1}{\alpha_r A_r})^{-1} \tag{8}$$

From the above calculation: the ΣR_i is the sum of heat conduction resistances through the pipe wall and fin. However, the frost formation upon the coil surface has not been considered in this paper due to the elevated secondary refrigerant inlet temperature.

When the heat exchanger outer surface temperature is below the dew point temperature of incoming air, dehumidification will occur.

The total heat transfer from airside for each element at (*i,j,k*) can be calculated as:

$$\dot{Q}_{tot} = \dot{m}_a(i,j,k) \times [h_a(i,j,k) - h_a(i,j+1,k)] \tag{9}$$

At dehumidification conditions,

18

$$h_a(i, j+1, k) = h_a(i, j, k) - \frac{\alpha_a A_o}{\dot{m}_a(i, j, k) \times C_{p,a}(i, j, k)} [h_a(i, j, k) - h_w(i, j, k)] \qquad (10)$$

The mass transfer of air at such conditions can be calculated as:

$$\omega_a(i, j+1, k) = \omega_a(i, j, k) - \frac{U_m A_o}{\dot{m}_a(i, j, k)} [\omega_a(i, j, k) - \omega_w(i, j, k)] \qquad (11)$$

The mass transfer coefficient U_m is determined by the Lewis correction:

$$U_m = \frac{\alpha_a}{C_{p,a}(i, j, k) \times Le^{2/3}} \qquad (12)$$

where the Lewis number, Le, is taken to be unity.

The parameters at grid points $(i+1, j, k)$ for the refrigerant and $(i, j+1, k)$ for the air can be obtained when all equations (4) to (12) collectively solved.

The accurate model prediction is dependent upon the precise calculation of fluid properties, heat transfer coefficients and pressure drops in both the refrigerant and air sides. The secondary refrigerant properties were calculated using the correlations from [25]. For the liquid secondary refrigerant, the calculation of the heat transfer coefficient for the refrigerant in-tube flow was derived from the Dittus-Boelter correlation [26]. Moreover, the Blasius equation [27]was used to calculate the required friction factor *f* in equation (5) and the air side heat transfer and friction coefficients were computed using the correlations from [28][29].

4.3 Integration model

The CFD model can be applied to simulate both air dynamics and heat and mass transfers for the air flow from the cooling coil air-off to air-on. It is expected to generate a precise prediction for the air flow performance, should the boundary condition at the cooling coil air-off be accurately defined. Conversely, the cooling coil model with a distributed model can also simulate the coil performance with a notable accuracy, assuming the cooling coil air-on parameters are provided correctly. Nonetheless, these airside boundary conditions vary with different operating states and therefore cannot be assumed accurately; therefore, the integration of the CFD and cooling coil models can simulate the actual performance of the display cabinet with a far greater accuracy.

The integration is developed through the connection of the models of the CFD and cooling coil under the simulation environment of TRNSYS [30], as shown in the block diagram of Figure 6. This simulation initiates from the CFD model with the implementation of various boundary parameters at the cooling coil air-off, including air velocity, dry-bulb temperature and relative humidity. However, the cooling coil model will not activate until the relative CFD model iterations are converged such that the total computing time for each iteration of the integrated model will be the sum of CFD and cooling coil models'. The outputs at the cooling coil air-on include air velocity, dry-bulb temperature and relative humidity will be extracted from the CFD model and used as inputs for the cooling coil model. Afterwards, the cooling coil model outputs at the air-off will renovate the boundary conditions of the CFD model and the simulation of the integrated model will continue until all the parameters at the component model inputs and outputs are converged. At the end, at each operating state, the total computation time for the integration model is approximately 10 to 15 minutes depending on computer speed.

Figure 6. Integration of the CFD and cooling coil models under the simulation environment of TRNSYS

5. Model validation

Overall, a total of five test conditions were designed and implemented for experimentation, of which chamber space temperatures were controlled to be a constant 25 °C, and the space air relative humidity varied between 30% and 70% with a 10% step increase. Throughout the experiment, the refrigerant mass flow rate, coil inlet refrigerant temperature and air mass flow rate remained unchanged in all test conditions at 0.245 kg/s, -5.5 °C and 0.44 kg/s respectively. The refrigerant coil inlet temperature was purposely controlled to be at a higher value than that of the manufacture designed value in order to prevent frost formation upon the external coil surface. At such conditions, the parameters were employed as inputs to the developed integration model of the display cabinet and the structure data of the cabinet and cooling coil (as introduced in Section 2) was used as the unchanged parameters for the model. The measurements collated at coil refrigerant outlet, the cooling coil air-on and air-off, and product simulators can be exploited in the validation of the developed model.

The simulation results at the typical ambient temperature of 25 °C and 50% relative humidity (mean values from the test) are shown in Figure 7 and Figure 8, with air and product temperature contours and air velocity vectors respectively. From the first

diagram, the air curtain and the heat exchange of its surroundings can be clearly identified, where the air curtain can be observed to have efficiently formed a heat exchange barrier between the internal cabinet and external environment. However, the products in close proximity to the sides of the air curtain have a relatively higher temperature than those nearer the back panel, due to the interaction between the air curtain and the cold perforated back panel flow. However, as shown in Figure 8, the space air temperature is affected solely by the right side of the air curtain due to air entrainment and spillages. The air entrainment from ambient space occurs in the upper regions of the air curtain and spillages in the lower, wherein this net effect provides the basis for the infiltration load to the display cabinet[9][31-32]. These scenarios will be similar for different operating states, with the exception of simulated parameter magnitudes.

Figure 7 Air and product temperature contours for ambient condition at temperature 25°C and 50% relative humidity

Figure 8 Air flow velocity vectors for ambient condition at temperature 25°C and 50% relative humidity

The graph in Figure 9 shows the simulation and test results for air temperatures at air-on and air-off and the refrigerant temperature at the coil exit in variation with space air

humidity. From this, the Figure ascertains that the air temperatures at either air-on or air-off increases alongside the refrigerant exit temperature with the higher space air relative humidity. The proliferation rate is relatively higher for lower air humidity regions. Subsequently, the simulation and test results correspond suitably. The air humidity at air-on and air-off were also predicted by the integrated model and compared to the test results, as shown in Figure 10, where the air humidity at either air-on or air-off is found to be enhanced with a higher space air relative humidity. With a space air humidity approaching 70%, the air humidity at air-off was not fully tested, although the simulation presented it to reach 100%, consequently attaining similar results for both the simulation and experimentation. When the air and refrigerant parameters at coil entry and exit were obtained from the simulation and test results, the calculations for the display cabinet total and sensible cooling loads can be conducted and compared, as illustrated in Figure 11, where more total cooling capacity is required with a higher space air relative humidity. However, the varied space air relative humidity does not influence the sensible cooling load. Accordingly, the accuracy of the model prediction comparisons can be deemed to be satisfactory.

Figure 9 Variation of air temperatures at air-on and air-off and refrigerant temperature at coil exit with various ambient relative humidity

Figure 10 Variation of air relative humidity at air-on and air-off with various ambient relative humidity

Figure 11 Variation of the cabinet cooling load with various ambient relative humidity

There were 11 products loaded onto the shelves at the middle section of the cabinet. As shown in Figure 1, these products are numbered in a sequence from 1 to 11, of which the product numbers 1,3,5,6,8 and 10 are product simulators with temperatures measured. The effect of ambient air humidity upon the product temperature were simulated and compared to the test results. The product temperature and surrounding air temperature contours with ambient humidity varying from 30% to 70% were predicted and shown in Figure 12, which ascertained that the temperatures of the product, air on and off all increased with a higher ambient humidity. The comparison between the predicted product temperatures and measurements at various space air humidity is illustrated in Figure 13 wherein product temperature for each condition increases in a sequence from number 1 to 11 and reaches a maximum value at 11. The product temperatures can thus be categorized into three separate levels according to their temperature scales: numbers 1 - 5, 6 - 10 and 11. Ideally, the maximum product temperature requires constant monitoring and control to ensure the designed maximum product temperature for the display cabinet not attained. The temperature for product number 2 is also established to be slightly lower than that of product number 1, due to the lower panel perforated rate near the 4th shelf where product number 1 is located. The interaction between the perforated back panel flow and the air curtain also instigates the product temperature for number 9 to be below that of number 8.

In accordance with the various test and simulation results, at a constant ambient temperature, refrigerant inlet condition and air flow rate, the product temperature has been found to increase with the ambient air humidity despite any raise in the cooling capacity requirement. Therefore, other control strategies for the limitation of the maximum product temperature require further exploration and analysis with the support of the validated model.

Figure 12 Product temperature contours with different space air relative humidity

Figure 13 Comparison of predicted product temperatures with test results at different space air relative humidity.

6. Model application

With the use of the validated integration model of the display cabinet, the exploration and analysis into alternative control strategies for the display cabinet using a secondary refrigerant at different operating states can be conducted. The varied operating parameters considered here are: space air temperature, space air humidity and cabinet circulate air flow rate. The preliminary consideration is respected when one of the above parameters is changed, in how to control the air temperature at cooling coil air-off to a specified value by modulating the refrigerant mass flow rate and maintaining the

refrigerant inlet temperature. The air temperature at the coil air-off and refrigerant inlet temperature are specified as 0 °C and -5.5°C respectively during the analyses.

6.1 Variation of space air temperature

In a modern supermarket, the space temperature is usually controlled to be constant, although the controlled value can be different dependent on the location of the supermarket. However, any change in the space air temperature will unquestionably affect the cabinet product temperature. Figure 14 shows the prediction of refrigerant mass flow rates to control air temperature at coil air-off of 0°C, at a constant space air humidity of 50%, cabinet air velocity of 1.2m/s and refrigerant inlet temperature of -5.5 °C when space air temperatures vary from 18 °C to 26 °C. The prerequisite cooling capacities are also calculated and illustrated in the same diagram to demonstrate that the maintenance of the constant air-off air temperature requires both the refrigerant mass flow rate and cooling capacity to increase with a higher space air temperature. A raise in the product temperature at each location is also observed along with a higher space air temperature, especially for the product numbers above 6, as shown in Figure 15. However, the product temperature is relatively lower than that without an air-off air temperature control.

Figure 14 Variation of refrigerant mass flow rate and required cooling capacity with space air temperature

Figure 15 Variation of product temperature with space air temperature

6.2 Variation of space air relative humidity

The collaborated test and simulation results of section 5 establish that at a constant space air temperature, cabinet air velocity and unchanged refrigerant inlet parameters, the air-off air temperature will increase along with a higher space air humidity to consequently raise the product temperature to an even greater extent. If the air-off air temperature is controlled to a specified lower value by modulating the refrigerant mass flow rate, the product temperature is expected to be suitably controlled. Accordingly, at a constant space air temperature of 25 °C, cabinet air velocity of 1.2m/s, refrigerant inlet temperature of -5.5 °C and controlled air temperature at coil air-off of 0°C, the refrigerant mass flow rates are predicted by the model when the space air humidity varies from 30% to 70% and illustrated in Figure 16. These simulation results verify that with higher space air humidity, the refrigerant mass flow rate and required cooling capacity both necessitate an increase so as to maintain the air-off air temperature. It is understood that the temperature of each product will not change with different space air humidity when the air-off air temperature is controlled. Furthermore, the maximum product temperature can be lower than that without air-off air temperature control and further reduced to any desired value through the adjustment of the setting point of the air-off air temperature.

Figure 16 Variation of refrigerant mass flow rate and required cooling capacity with space air humidity

6.3 Variation of cabinet air flow velocity

The cabinet air flow velocity is another important parameter which requires regulation at the design stage for a specified display cabinet. To illustrate the design procedure, the design condition assumed in the paper has a 25 °C space air temperature, 50% space air humidity and -5.5 °C refrigerant inlet temperature. The modulated refrigerant mass flow rate is subsequently predicted by the model in order to control the air-off air temperature at 0 °C when the air velocity increases from 0.8m/s to 1.6 m/s, as shown in Figure 17. As expected, both the refrigerant mass flow rate and cooling capacity require an increase with the higher cabinet air velocity in order to control the specified air-off air temperature. Simultaneously, the product temperatures simulated with the increased air velocity is shown in Figure 18 where each product temperature reduces with a higher cabinet air velocity. The designed cabinet air velocity can thus be retained for a specified cabinet cooling capacity and a designated maximum product temperature.

Figure 17 Variation of refrigerant mass flow rate and required cooling capacity with cabinet air velocity

Figure 18 Variation of product temperature with cabinet air velocity

7. Conclusions

A simulation model for the multi-deck medium temperature display cabinets has been developed through the integration of CFD air dynamic and detailed cooling coil sub-models. The integrated model is expected to be more accurate in predicting cabinet performance at different operating states compared to those utilising solely a separated CFD or cooling coil model. This developed model has also been validated together with test results at varied space air humidity and can therefore be used to explore and analyse the optimal designs of the geometrical structures of cabinets, curtains and coils and further of control strategies and operating states for the cabinets. These test and simulation results established that at a constant space air temperature, cabinet air velocity and unchanged refrigerant inlet condition, both the air-off air temperature and required cooling capacity increased with higher space air humidity. Consequently, each product temperature in the cabinet increases accordingly. However, since the maximum product temperature may mount higher than the permitted value for the highest space air humidity, the air-off air temperature therefore requires careful control to a specified lower value through modulating the refrigerant mass flow rate. For this paper, the controlled air-off air temperature is set to 0°C, although, in practice, this can be adjusted to meet the requirement of the desired maximum product temperature. Moreover, with the control of the air-off air temperature, the product temperature will not be affected by changing space air humidity, and the maximum product temperature can thus be ably managed. It is also found that, although the product temperature still increases with a higher space air temperature, the maximum product temperature can be reduced when

the air-off air temperature is controlled. Furthermore, should the cabinet air velocity increase at the restraint of the air-off air temperature, both the refrigerant mass flow rate and prerequisite cooling capacity would necessitate an augmentation along with the reduced product temperature, which proves to not be obligatory. Ultimately, the required cabinet air velocity at the designed operating state can effectively be determined.

Acknowledgements

References

[1] Faramarzi R. Efficient display case refrigeration. ASHRAE J, November 1999. p. 46-54.

[2] Tassou SA. Potential for solar energy in food manufacturing, distribution and retrail, Report to DEFRA, AC045; 2007 [25 p.].

[3] Howwell RH, Van NH, Smith CE. Heat and moisture transfer through recirculated plane air curtains. ASHRAE Trans 1976;82(1):191–205.

[4]   Howell RH, Shiabata M. Optimum heat transfer through turbulent recirculated plane air curtains. ASHRAE Trans 1980;86(1):188–200.

[5]   Howell RH, Adams PA. Effects of indoor space conditions on refrigerated display case performance. ASHRAE Research Project 596-RP, Department of Mechanical Engineering, University of South Florida, Tampa, 1991.

[6]   Ge YT, Tassou SA. Modelling the performance of single jet air curtain in open refrigerated display cabinets. J Appl Therm Eng 2001;21(2):201–19.

[7]   Smale NJ, Moureh J, Cortella G. A review of numerical models of airflow in refrigerated food applications. International Journal of Refrigeration 2006; 29,911-930.

[8]   Stribling D, Tassou SA, Mariott D. A two-dimensional CFD model of a refrigerated display case. ASHRAE Trans 1997;103(1):88–94.

[9]   Cortella G. CFD-aided retail cabinets design. Computers and Electronics in Agriculture 2002;34, 43-66.

[10]   D'Agaro P, Cortella G, Croce G. Two- and three-dimensional CFD applied to vertical display cabinets simulation. International Journal of Refrigeration 2006; 29, 178-190.

[11]   Foster AM, Swain MJ, Barret R, D'Agaro P. Three-dimentional effects of an air curtain used to restrict cold room infiltration. Applied mathematical Modelling 2007;31,1109-1123.

[12]   Foster AM, Madge M, Evans JA, The use of CFD to improve the performance of a chilled multi-deck retail display cabinet. International Journal of Refrigeration 2005; 28 ,698–705.

[13]   Navaz HK, Ramin F, Dabiri D, Gharib M, and Modarress D, The application of advanced methods in analysing the performance of the air curtain in a refrigerated display case. Journal of Fluid Engineering 2002; 124:756-764.

[14]   Navaz HK, Henderson BS, Faramari R, A. Pourmovahed, F. Taugwalder, Jet entrainment rate in air curtain of open refrigerated display cases. International Journal of Refrigeration 2006; 29: 178-190.

[15] Navaz HK, Dabiri D, Amin M, and Faramarzi R, Past, present, and future research toward air curtain performance optimization. ASHRAE Transactions 2005; 111(1): 1083-1088.

[16]   Chandrasekharan R, Verma P, Bullard CW, Development of a design tool for display case evaporators. International Journal of Refrigeration 2006;29: 823-832.

[17] Getu HM, Bansal PK, Modelling and performance analyses of evaporators in frozen-food supermarket display cabinets at low temperatures. International Journal of Refrigeration 2007; 30 :1227-1243.

[18] Domanski PA, Vance PW, Properties and cycle performance of refrigerant blends operating near and above the refrigerant critical point, Task2: air conditioner system study. 2002; Final report, October.

[19] Tso CP, Cheng YC, Lai AC, Dynamic behavior of a direct expansionevaporator under frosting condition, Part I. Distributed model, International Journal of Refrigeration 2006;29: 611-623.

[20] Wang FQ, Maidment GG, Missenden JF, Tozer RM, A novel special distributed method for dynamic refrigeration system simulation. International Journal of Refrigeration 2007;30: 887-903.

[21] Launder BE, Spalding DB, The numerical computation of turbulent flows. Comput. Methods Appl. Mech. Engrg. 1974; 3: 269-289.

[22] Xiang WZ. Performance improvement of multi-deck display cabinets and reduction of their impact on the store environment. PhD thesis, Brunel University 2003.

[23] Patankar SV, Spalding DB, A calculation procedure for heat, mass and momentum transfer in three-dimensional parabolic flows. International Journal of Heat Mass Transfer 1972; 15:1787–1806.

[24] Kays WM, London AL. *Compact heat exchangers*, 3rd ed. McGraw- Hill, New York. 1984.

[25] Melinder A, Thermophysical properties of liquid secondary refrigerants. International Institute of Refrigeration 1997.

[26] Incoprera FP, DeWitt DP, Fundamentals of Heat and Mass Transfer (John Wiley, New York), 1990.

[27] Incropera F.P., DeWitt DP, Introduction to heat transfer. 3rd ed. New York:John Wiley &Sons, 1996.

[28] Wang CC, Jang JY, Chiou NF, A heat transfer and friction correlation for wavy fin-and-tube heat exchangers. International Journal of Heat Mass Transfer 1999a; 42:1919-1924.

[29] Wang CC, Lee WS, Sheu WJ, A comparative study of compact enhanced fin-and-tube heat exchangers. International Journal of Heat Mass Transfer 2001; 44: 3565-3573.

[30] TRNSYS, A Transient System Simulation program, TRNSYS 16, 2005.

[31] Flick D, Moureh J, Ding Y. Confinement thermique d'une enceinte par jet d'air en convection forcée. Revue générale de thermique 1997; 36: 443-452.

[32] Moureh J, Ding Y, Flick D. Caractérisation expérimentale et numérique des transferts de chaleur à travers un jet d'air plan horizontal. 1996, Revue générale de Thermique 1996;35(415):469-474.
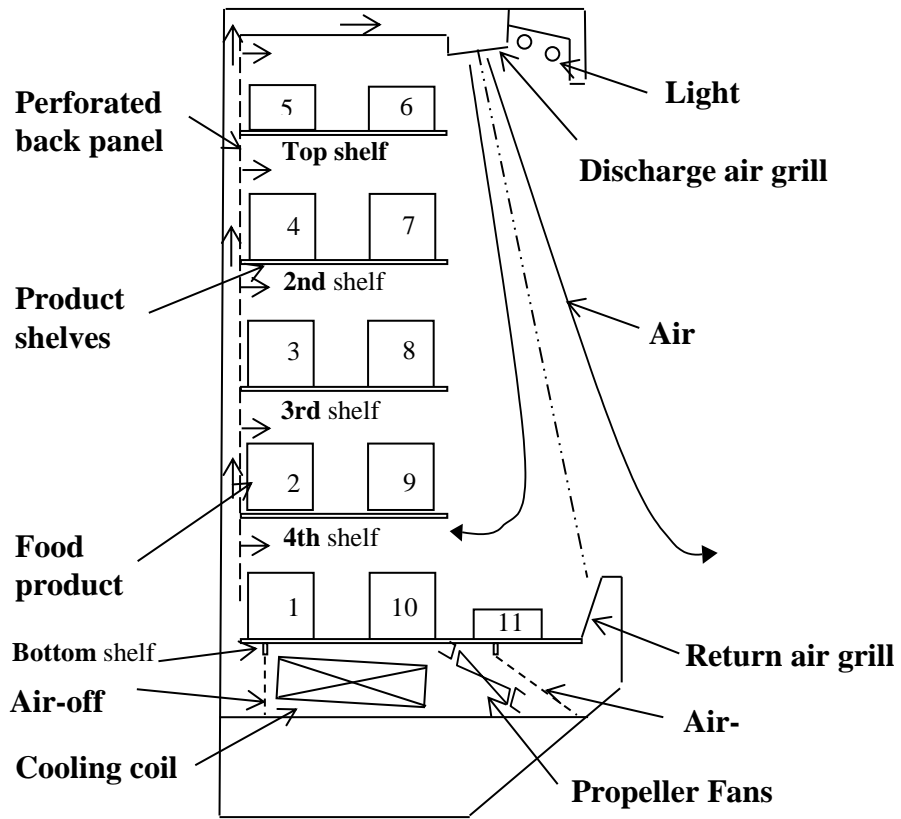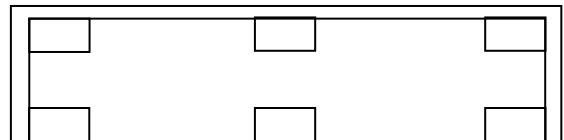
Figure 1 Tested Carter display cabinet

Figure 2.   The cooling coil in the tested display cabinet

Top shelf

2nd shelf

3rd shelf

4th shelf

Bottom shelf
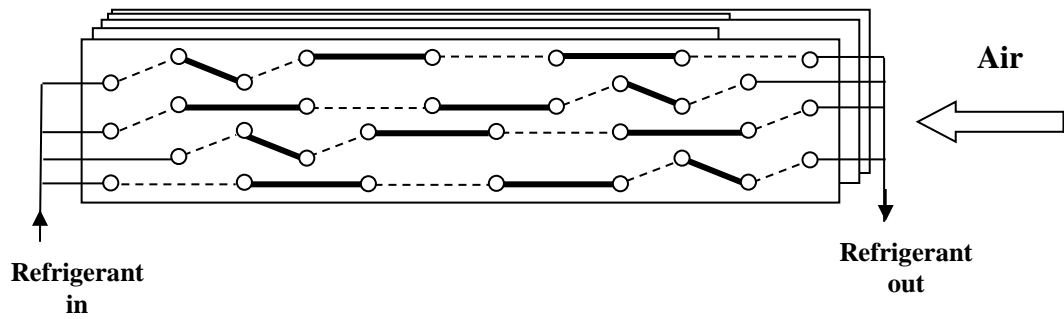
Left   Middl   Right
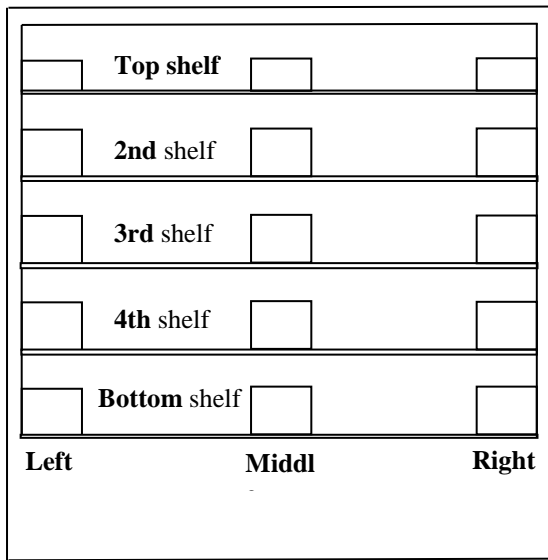
Front view of the tested display cabinet

Top view of the measurement shelf for the
tested display cabinet

Figure 3. Locations of product simulators inside the display cabinet

Table 1. Specifications and data descriptions of sensors used in the experiment

Sensor type	Make/Model	Data description	Accuracy
Temperature (RTD)	SEM105P	Chamber air temperature	± 0.1 °C
Humidity	SEM105H-3	Chamber air relative humidity	± 3 %
Temperature (TC)	T (Welded Tip Thermocouple PTFE insulated)	Air at coil air-on	± 0.2°C
		Air at coil air-off	
		Refrigerant at coil inlet	
		Refrigerant at coil outlet	
		Product simulators	
Refrigerant mass flow rate	Model KROHNE IFC 010D	Refrigerant mass flow rate in coil	0.2 %
Velometer	VelociCalc Plus meter	Air velocity at back panel tunnel inlet	± 0.015 m/s
Pressure	OMGA Model PX771A-100DI	Refrigerant pressure drop of coil	± 3 Pa
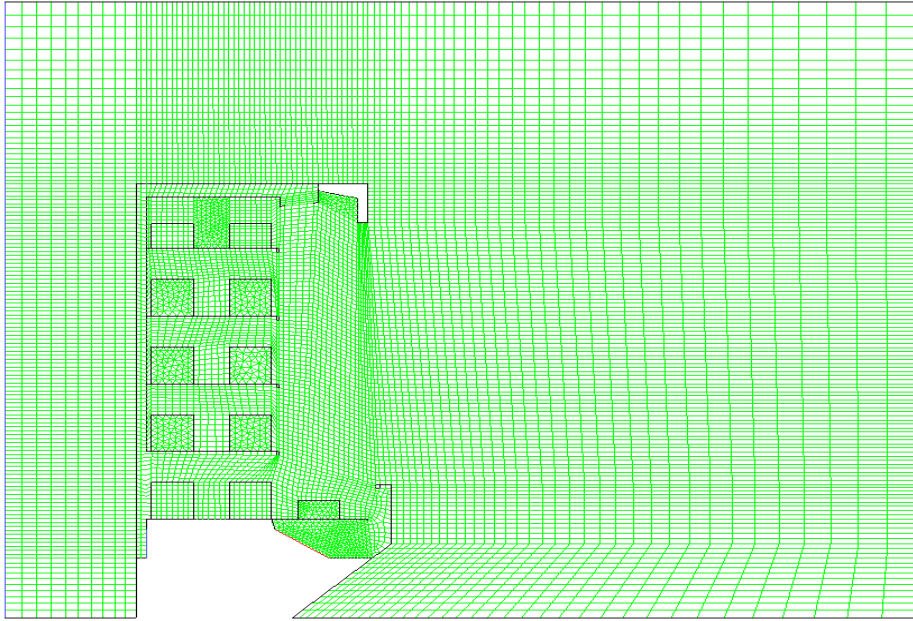
Figure 4 Computational grids for the 2D CFD model
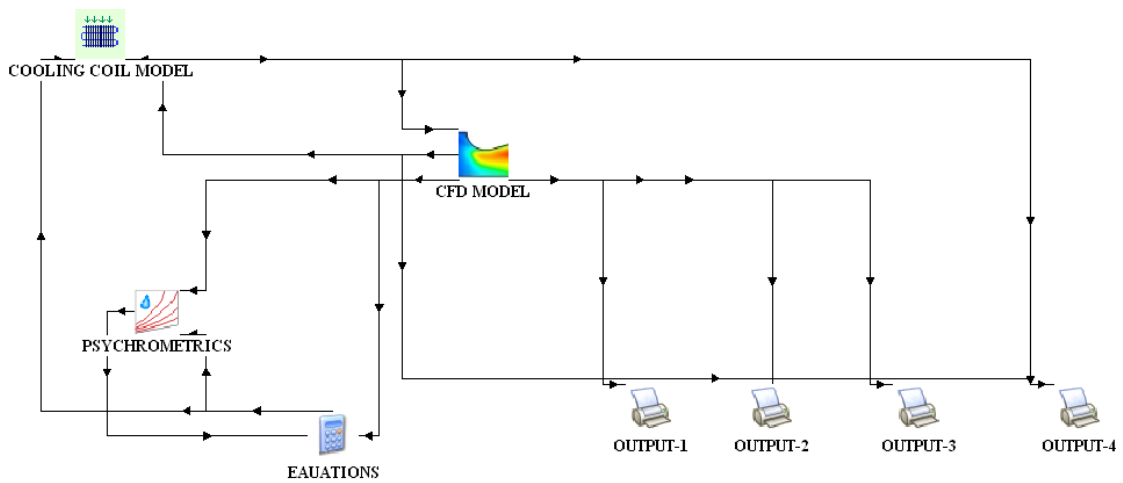
Figure 5. A sample air-cooling heat exchanger and coordination of the divided small element

Figure 6. Integration of the CFD and cooling coil models under the simulation environment of TRNSYS

| 2.98e+02 |
| 2.97e+02 |
| 2.97e+02 |
| 2.96e+02 |
| 2.95e+02 |
| 2.94e+02 |
| 2.93e+02 |
| 2.92e+02 |
| 2.92e+02 |
| 2.91e+02 |
| 2.90e+02 |
| 2.89e+02 |
| 2.88e+02 |
| 2.87e+02 |
| 2.87e+02 |
| 2.86e+02 |
| 2.85e+02 |
| 2.84e+02 |
| 2.83e+02 |
| 2.83e+02 |
| 2.82e+02 |
| 2.81e+02 |
| 2.80e+02 |
| 2.79e+02 |
| 2.78e+02 |
| 2.78e+02 |
| 2.77e+02 |
| 2.76e+02 |
| 2.75e+02 |
| 2.74e+02 |
| 2.74e+02 |
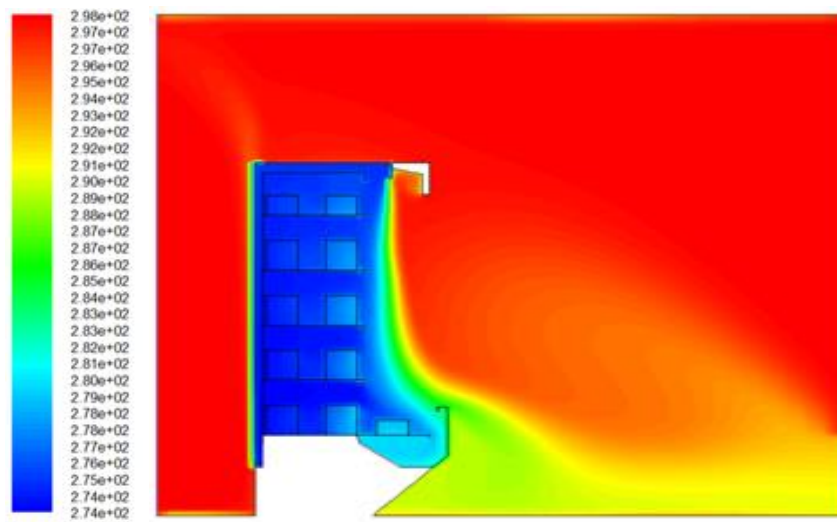
Figure 7 Air and product temperature contours for ambient condition at temperature 25°C and 50% relative humidity
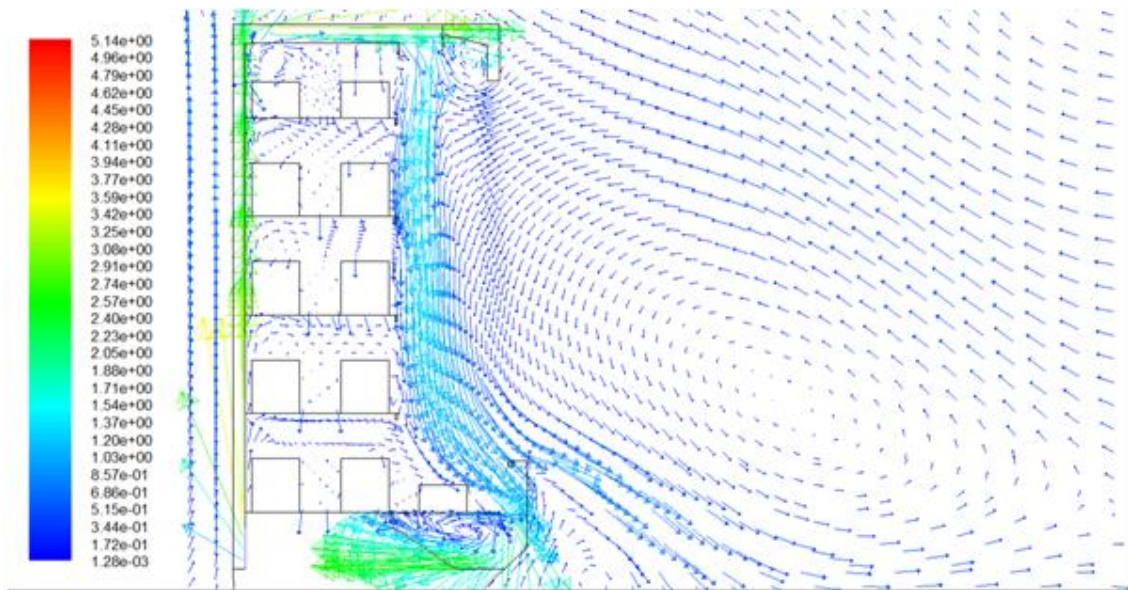
Figure 8 Air flow velocity vectors for ambient condition at temperature 25°C and 50% relative humidity
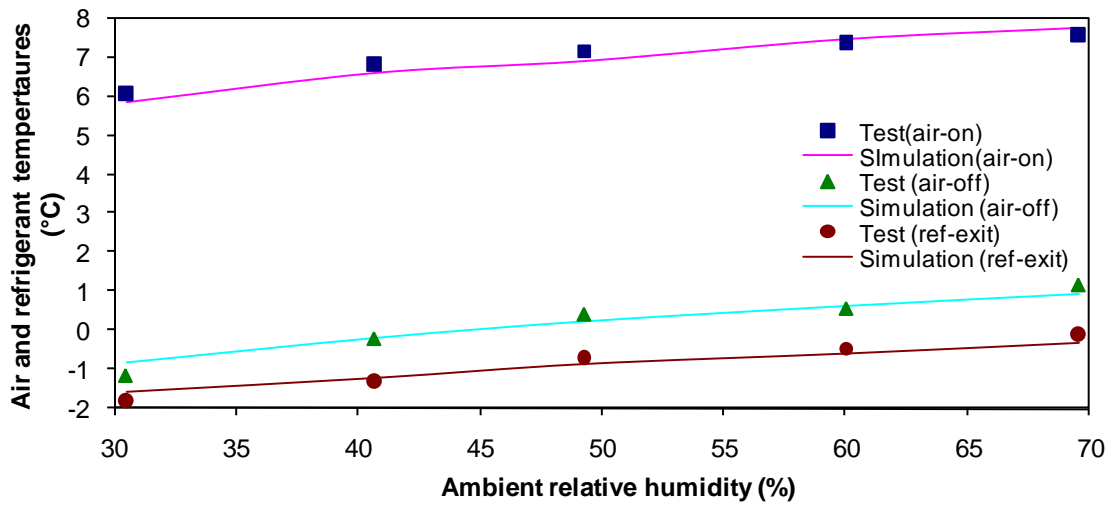
Figure 9 Variation of air temperatures at air-on and air-off and refrigerant temperature at coil exit with various ambient relative humidity
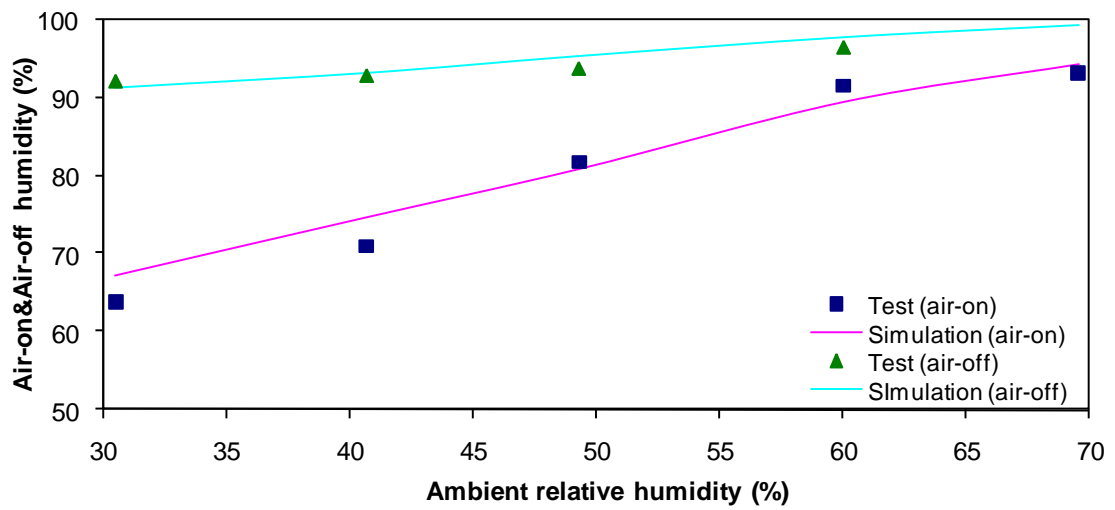
Figure 10 Variation of air relative humidity at air-on and air-off with various ambient relative humidity
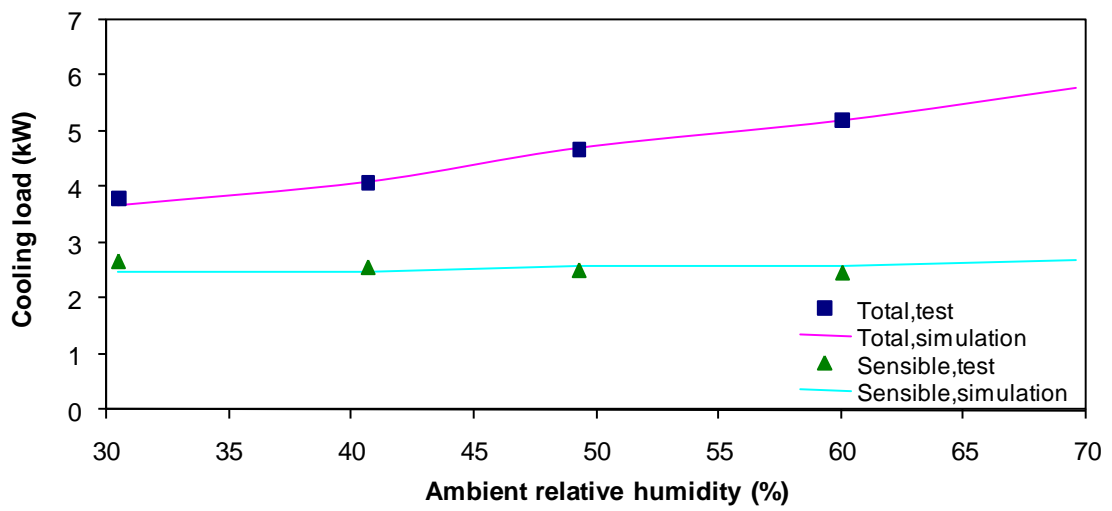
Figure 11 Variation of the cabinet cooling load with various ambient relative humidity
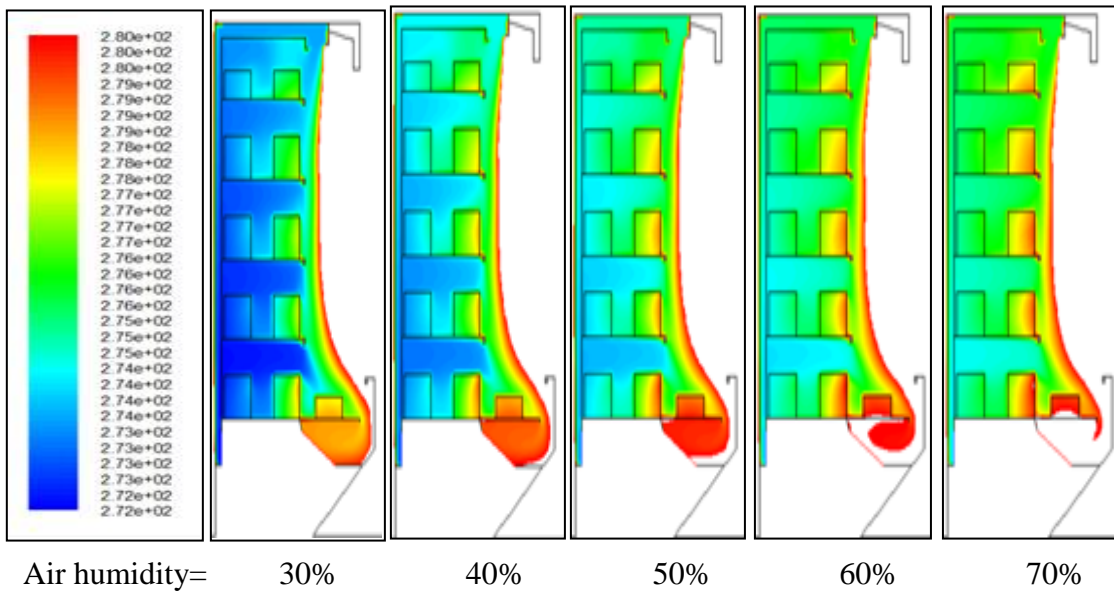
Figure 12 Product temperature contours with different space air relative humidity
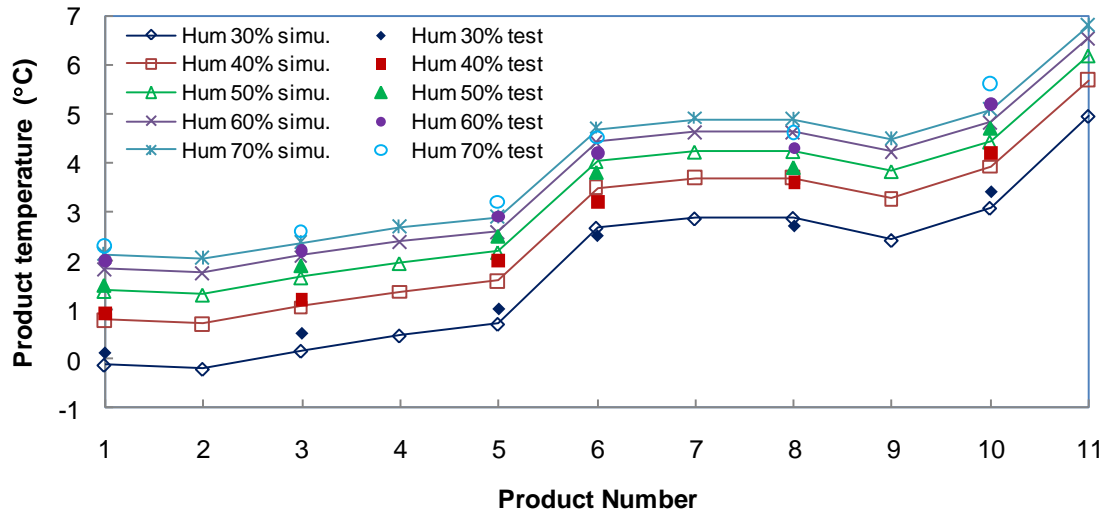
Figure 13 Comparison of predicted product temperatures with test results at different space air relative humidity.
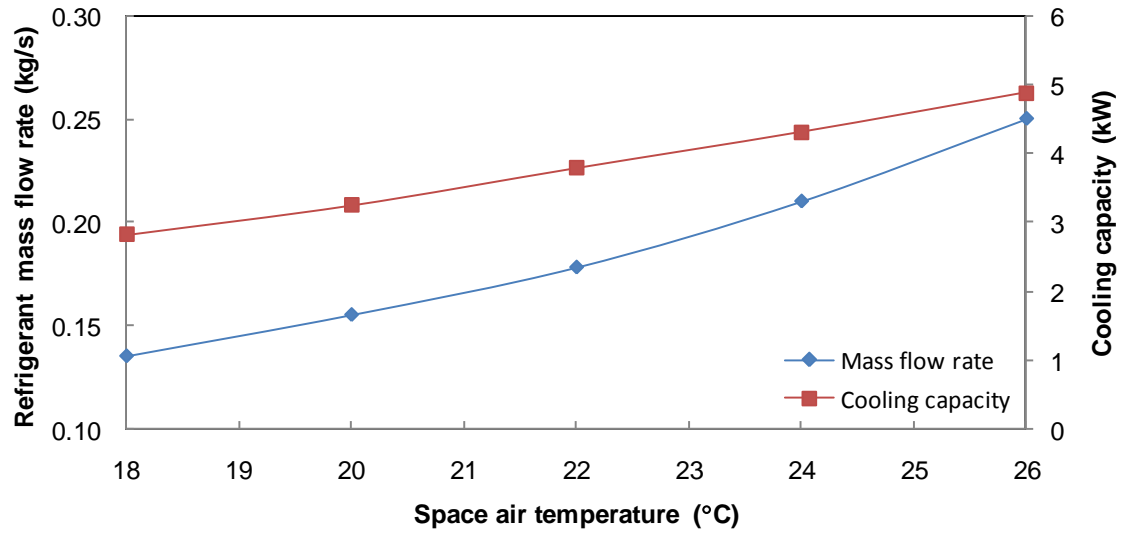
Figure 14 Variation of refrigerant mass flow rate and required cooling capacity with space air temperature
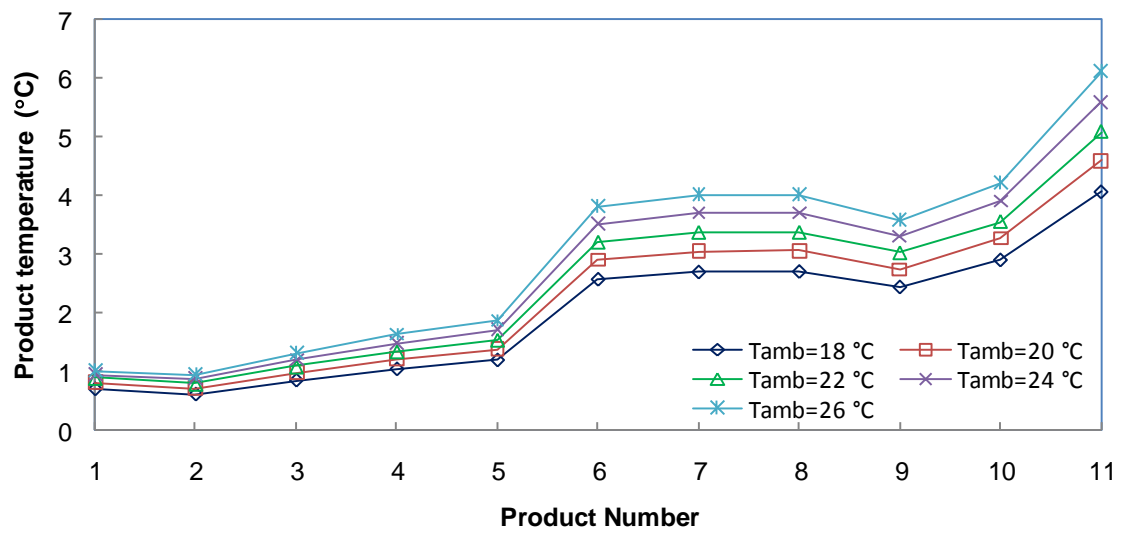
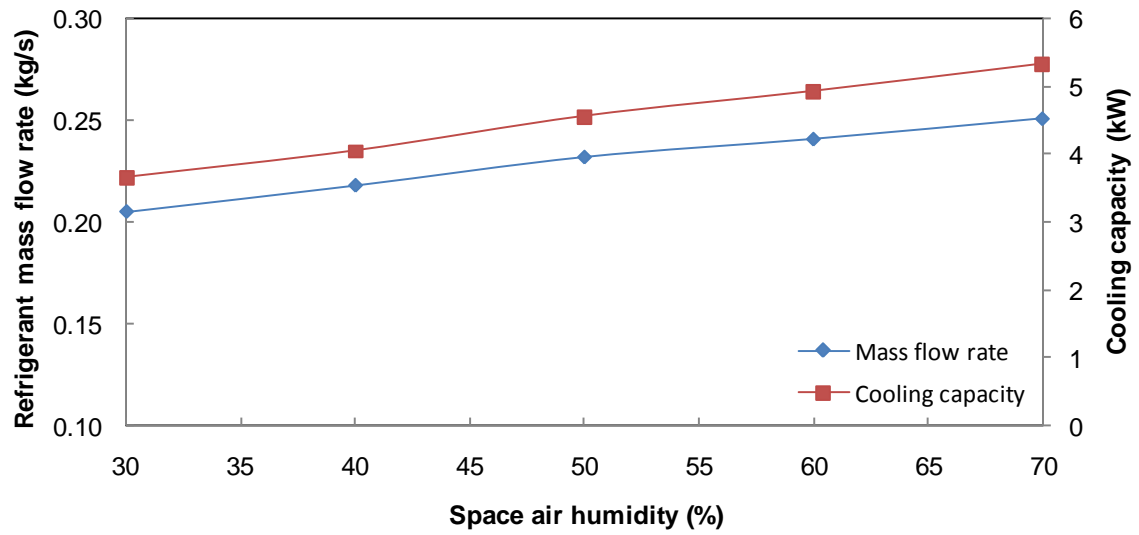Figure 15 Variation of product temperature with space air temperature

Figure 16 Variation of refrigerant mass flow rate and required cooling capacity with space air humidity
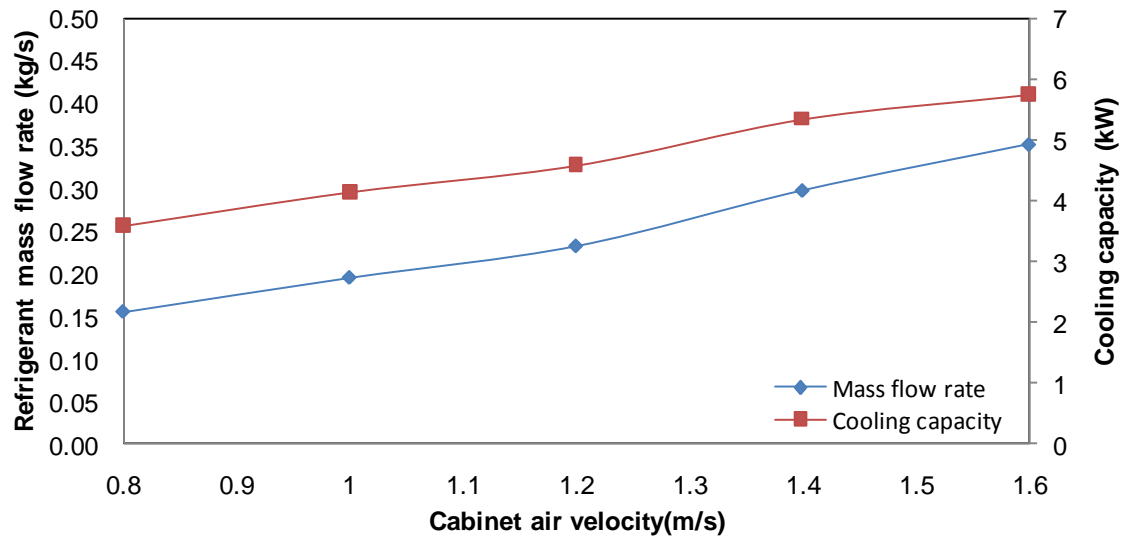
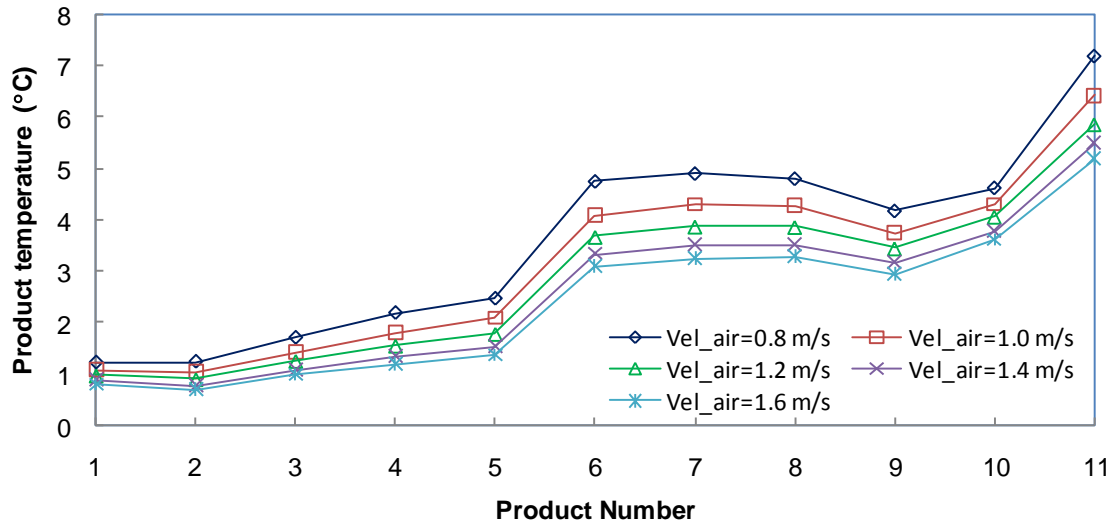Figure 17 Variation of refrigerant mass flow rate and required cooling capacity with cabinet air velocity

Figure 18 Variation of product temperature with cabinet air velocity